

The Effects of Cu and Zn Dopants on Phase Constituents, Magnetic Properties and Microstructure of Nickel Ferrite

S. Alamolhoda, S. M. Mirkazemi*, N. Benvidi and T. Shahjooyi

School of Metallurgy and Materials Engineering, Iran University of Science & Technology (IUST), Narmak, Tehran 13114-16846, Iran

(*) Corresponding author: mirkazemi@iust.ac.ir
(Received: 23 August 2015 and Accepted: 03 July 2016)

Abstract

In this research nanoparticles of $Ni_{0.55}Zn_{0.35}Cu_{0.1}Fe_2O_4$ were synthesized by sol-gel auto-combustion method. Changes in phase constituents, microstructure and magnetic properties as a result of Zn and Cu additions were evaluated by X-ray diffraction (XRD), Field Emission Scanning Electron Microscope (FESEM), and Vibration Sample Magnetometer (VSM) techniques. XRD results show that the doped sample have a single phase cubic spinel structure while the undoped sample consists of $NiFe_2O_4$, $FeNi_3$, $\alpha-Fe_2O_3$ and NiO phases. Changes in cell parameter calculated by MAUD software using XRD patterns showed that the cell parameters of the doped sample had expansion about 0.044 \AA . Microstructural studies demonstrated considerable reduction of particle size and particle size distribution in the sample synthesized with dopants. Magnetic measurements have been determined increasing of the saturation magnetization from 36.96 emu/g to 56.46 emu/g and decreasing of coercivity force from 175.50 Oe to 98.79 Oe in the sample synthesized with dopants. Changes in microstructure and magnetic properties have been explained.

Keywords: Nickel ferrite, Sol-gel auto-combustion, Magnetic properties, Dopants, Nanoparticles.

1. INTRODUCTION

Synthesis and application of nanomaterials is the subject of most researches because of their unique physical and chemical properties [1]. Chemically synthesized magnetic nanoparticles recently have been attracted much attention due to their unique magnetic properties derived from their small particle size and uniform size distribution [2, 3]. Nanoparticles of nickel ferrite as one of the most common spinel ferrites has been widely studied due to its high electro-magnetic performance, excellent chemical stability and mechanical hardness, high coercivity and moderate saturation magnetization. These properties make this material suitable for applications as magnetic drug delivery, magnetic information storage device, ferrofluids, sensors, catalysis, soft magnets and low

loss materials at high frequencies [4-6]. Unlike the metallic magnetic materials, nanoparticles of nickel ferrite display low eddy current loss in alternating current applications as a result of relatively low electrical conductivity and they are particularly useful in the radio frequency range [7]. Nickel ferrite nanoparticles have been prepared by several methods such as co-precipitation [8], hydrothermal [9], sol-gel [2] and sol-gel auto-combustion [10]. Among these methods sol-gel auto-combustion is a facile and cost effective method. It provides low temperature processing and molecular level mixing of materials and the produced product is a fine and homogeneous powder [11, 12]. Tetrahedral sites of inverse spinel structure of $NiFe_2O_4$ are occupied by ferric ions while the octahedral sites are occupied by

both ferric and nickel ions [13]. By substitution of dopant ions in the inverse spinel structure, depending on site occupancy of the ions in tetrahedral or octahedral sites the structural, the electrical and magnetic properties of the base material would be changed [7, 14 and 15]. NiZn ferrite is a magnetic material that has wide applications in high and low frequency and microwave equipment. NiZn ferrite is a mixed spinel in which the tetrahedral sites are occupied with Zn^{2+} and Fe^{3+} ion and the octahedral sites are occupied with Ni^{2+} and Fe^{3+} ions. However it should be noted that the site occupancy of different ions in tetrahedral and octahedral sites would be changed with the sintering temperature and particle size of the synthesized ferrites [16]. Copper addition in the ferrites was also investigated. It was observed that copper addition causes interesting electrical and magnetic properties [17]. In this research the effects of Cu and Zn dopants on magnetic properties and microstructure of the nickel ferrite synthesized by sol-gel auto combustion method with the aim of application at high frequency and microwave equipment were investigated.

2. MATERIALS AND METHODS

In order to prepare $NiFe_2O_4$, 7.35g $Fe(NO_3)_3 \cdot 9H_2O$ (99% Merck) and 2.56 g $Ni(NO_3)_2 \cdot 6H_2O$ (99% Merck) were dissolved into 50 ml distilled water to make an aqueous solution. Then 5.25g citric acid ($C_6H_8O_7$, 99% Merck) was added to the above mixture as a chelating agent with a nitrate to citrate ratio of 1:1. The solution was heated at 60°C on magnetic stirrer with a rotating speed of 300rpm to form a clear and green sol with $pH < 1$. The pH value of the solution was raised to 7 by addition of ammonia solution. The resulting sol was heated at constant temperature of 80°C on magnetic stirrer to complete the reaction for forming the gel precursor. Then the gel undergoes a self-ignition reaction to form a very fine brown foamy powder. In order to prepare

$Ni_{0.55}Zn_{0.35}Cu_{0.1}Fe_2O_4$ compound 7.64g $Fe(NO_3)_3 \cdot 9H_2O$ (99% Merck), 1.51 g $Ni(NO_3)_2 \cdot 6H_2O$ (99% Merck), 0.73g $C_4H_6O_4Zn \cdot 2H_2O$ (98% Merck) and $CuCl_2 \cdot 2H_2O$ (98% Merck) were dissolved into 50 ml distilled water and the same process as mentioned above was repeated for this sample. $Ni_{0.55}Zn_{0.35}Cu_{0.1}Fe_2O_4$ compound was named "NCZ" and undoped sample was named "N".

The phase identification of the combustion products were performed by Philips X'pert Pro X-ray diffractometer (XRD) using $Cu K\alpha$ radiation ($\lambda = 0.1541$ nm). The XRD patterns were submitted to a quantitative analysis by the Rietveld method using MAUD (material analysis using diffraction) software [18]. The mean crystallite size and lattice strain of the particles were calculated using Williamson-Hall equation:

$$\beta \cos \theta = \lambda / D + 4 \varepsilon \sin \theta \quad (1)$$

Where D is the mean crystallite size, λ is the X-ray wavelength, β is the value of the full width at half maximum of the diffraction peaks, θ is the diffraction angle and ε is the lattice strain. A straight line would be drawn between $\beta \cos \theta$ versus $4 \sin \theta$. The slope of the line gives the lattice strain.

The morphology and microstructure of the nanoparticles were studied by a TESCAN (FESEM) model MIRA. Magnetic properties were taken out at room temperature at the maximum applied field of 14kOe by vibrating sample magnetometer (VSM) model MDK.

3. RESULTS AND DISCUSSION

XRD patterns of the combustion products of the samples N and NCZ are shown in Figure 1. According to the XRD results sample N consists of $NiFe_2O_4$ as the main phase coexisting with α - Fe_2O_3 and $FeNi_3$ phases. Presence of NiO phase is also possible in the combustion product since NiO XRD peaks overlap with the peaks of $NiFe_2O_4$. In another paper presence of NiO was shown by Raman spectra of the combustion product [10].

XRD pattern of sample NCZ showed single phase doped nickel ferrite and α -Fe₂O₃ and FeNi₃ phases were not observed. Figure 2 shows XRD peaks of sample NCZ and standard reference patterns of NiFe₂O₄ and NiO phases. It could be observed that the intensity of the sample peaks is nearly the same as the standard peaks of nickel ferrite. So unlike the sample N, the sample NCZ might be single phase.

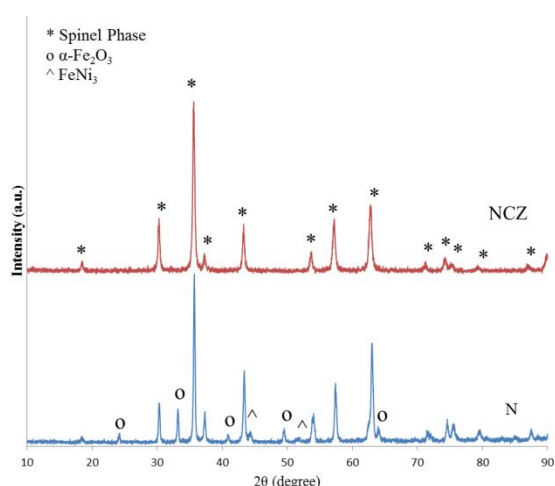


Figure 1. XRD patterns of the samples N and NCZ.

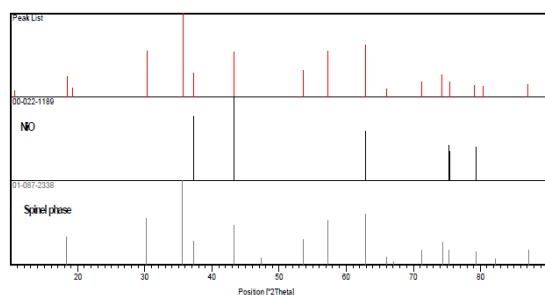


Figure 2. XRD peaks of sample NCZ and standard reference patterns of NiO.

Formation of single phase nickel ferrite in sample NCZ might be due to Cu and Zn substitution in the tetrahedral and octahedral sites in the spinel structure. In order to substitute a cation in the structure with another one their ionic radius must be near each other and their structure should be the same. The ionic radius of Cu²⁺ and Zn²⁺ are equal to 0.72Å and 0.74Å respectively which are close to the ionic radius of Ni²⁺ 0.69 Å. Therefore

substitution of these dopants is probable in the spinel structure [16]. Calculations with MAUD software demonstrates that this substitution causes increment of lattice constant from 8.345 Å in sample N to 8.389 Å in sample NCZ.

The plotted lines between $\beta\cos\theta$ versus $4\sin\theta$ for samples N and NCZ are shown in Figure 3. The mean crystallite sizes of the synthesized nickel ferrite in samples N and NCZ which were calculated with Williamson-Hall formula (using polts in Figure 3) are equal to 62 and 36 nm respectively, representing reduction of crystallite size using Cu and Zn dopants. The calculated strain value for both samples were the same and nearly equal to 0.0018 which is due to similarity of the ionic radii of Cu²⁺ and Zn²⁺ to the ionic Ni²⁺ radius.

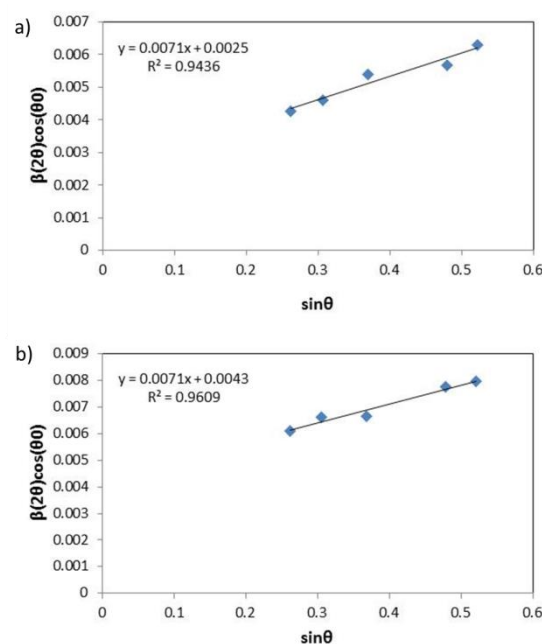


Figure 3. The plotted lines between $\beta\cos\theta$ versus $4\sin\theta$ for samples N and NCZ.

Figure 4 shows FESEM micrographs of samples N and NCZ. It could be observed that using Cu and Zn substitutions the particle size is considerably reduced. The morphology of the particles is also changed from sharp cornered to nearly spherical shaped. The reduced particle size demonstrates that the incorporation of

dopants in the nickel ferrite could increase the number of nucleation sites [19]. In addition the substituted cations may play the role of growth inhibitors in the combustion process [20]. Nearly spherical particle morphology also exhibits that the particle growth rate in all directions were the same. This means that presence of these substituted cations prevents from particle growth in some directions [21].

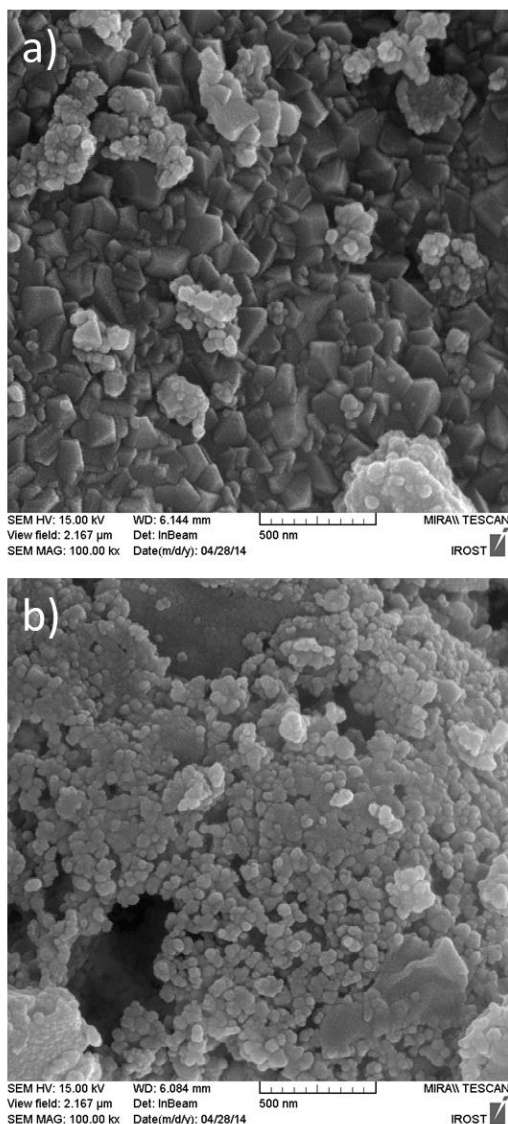


Figure 4. FESEM micrographs of samples a) N and b) NCZ.

Figure 5 shows magnetization curves of the samples N and NCZ. Table 1 also shows magnetic parameters of these samples. It could be observed that M_s value of the sample is increased from

39.35 emu/g to 56.46 emu/g using Cu and Zn dopants. The M_s value of nickel ferrite nanoparticles were reported to be equal to 50.4 and 46.5 emu/g [12, 22]. Therefore using Cu and Zn dopants increases the M_s value higher than the reported values for nickel ferrite nanoparticles.

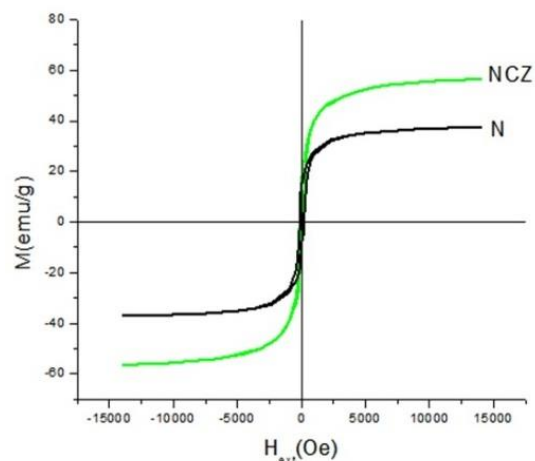


Figure 5. Magnetization curves of the samples N and NCZ.

Table 1. Magnetic parameters of the samples N and NCZ.

Sample	M_s (emu/g)	iH_c (Oe)	M_r (emu/g)
N	39.35	178.61	14.86
NCZ	56.46	98.79	11.74

Half of the Fe^{3+} ions occupy all of the tetrahedral sites and rest of them occupies half of the octahedral sites in the sample with no substituents [23]. According to the Neel's theory of ferrimagnetism, in the spinel structure the cations on different sublattices (tetrahedral and octahedral sites), have oppositely aligned magnetic moments [24]. Therefore the magnetic moment per formula unit (n_B) in the μ_B units is:

$$n_B = M_{oct} - M_{tet} \quad (2)$$

Where M_{oct} and M_{tet} are the magnetic moments of octahedral and tetrahedral sites, respectively. Ionic magnetic moment of Zn^{2+} , Cu^{2+} , Ni^{2+} and Fe^{3+} are equal to 0, 1, 2, 5 (μ_B) respectively [25]. Magnetic moments of Fe^{3+} ions neutralize each other

in the inverse spinel structure of nickel ferrite. Therefore the magnetic moment of the structure is the magnetic moment of Ni^{2+} ions. Nickel and zinc ferrites have inverse spinel structures and copper ferrite have normal spinel structure. Therefore the Zn^{2+} ions substitute Fe^{3+} ions in the tetrahedral sites. This increases the concentration of Fe^{3+} ions in octahedral sites and so increases the magnetization in the octahedral sublattice which changes the net momentum and enhances the M_s value. Also formation of ZnFe_2O_4 is probable since the XRD peaks of this phase overlap with nickel ferrite peaks and are not recognizable. Presence of ZnFe_2O_4 can affect the M_s value.

Cu ions substitute for the Ni ions. However during the formation of spinel lattice Ni ions occupy the tetrahedral sites; therefore the added Cu ions may occupy both octahedral and tetrahedral sites. In this case a fraction of Fe ions that are present at tetrahedral sites are forced to migrate to octahedral sites. This arrangement results in an increase in the magnetic moment of octahedral sublattice as the Fe^{3+} ions have a higher magnetic moment ($5\mu\text{B}$) than the Cu^{2+} ions which they replace, while that of the tetrahedral sublattice decreases. This leads to an increase in the magnetization, of the ferrite [26].

Coercivity force was about 178 Oe in sample N which was decreased to 98 Oe in the single phase sample that was synthesized using Cu and Zn dopants. iH_c values are much larger than the bulk ($iH_c = 10$ Oe). The mechanism has been explained in terms of spin-disorder, spin-canting, and spin-glass-like state in surface layers of nanoparticles due to local chemical disorder, broken exchange

interaction, and a dissimilar local symmetry for those atoms near the surface. Moreover, the surface barrier potential is enhanced because of the distortion of crystal lattice caused by the atoms deviate from normal positions in the surface layers. All these lead to a higher iH_c value [27]. The iH_c is inversely proportional to M_s according to Brown's relation. The amount of Ni^{2+} ions decreases as a result of presence of Cu and Zn dopants. This means that the magneto-anisotropy constant decreases with addition of dopants and consequently the magnitude of iH_c decreases [28].

4. CONCLUSION

Nanoparticles of $\text{Ni}_{0.55}\text{Zn}_{0.35}\text{Cu}_{0.1}\text{Fe}_2\text{O}_4$ were synthesized by sol-gel auto-combustion route. XRD results showed that formation of single phase nickel ferrite in the combustion product with Zn and Cu substitutions; while the combustion product of the undoped sample consisted of lateral phases such as hematite, Fe_2O_3 and NiO. Calculations using XRD result and MAUD software showed increasing of cell parameter (a) from 8.345 \AA to 8.389 \AA with Cu and Zn substitutions. FESEM micrographs showed considerable reduction of particle size in the sample synthesized with Cu and Zn dopants. This reduction might be due to the role of dopants in increasing of the mean path between other ions in the sol and inhibiting the growth of the particles during the combustion process. VSM results showed that M_s value increased from 36.96 emu/g to 56.46 emu/g while coercivity force value decreases from 175.5 Oe to 98.79 Oe using Cu and Zn substitutions.

REFERENCES

1. Ghasemi, A., Davarpanah, A. M., Ghadiri, M. (2010). "Structure and Magnetic Properties of Oxide Nanoparticles of Fe-Co-Ni Synthesized by Co-Precipitation Method", *Int. J. Nanosci. Nanotechnol.*, 8: 207-214.
2. Liu, X. M., Fu, S. Y., Huang, C. J. (2004). "Magnetic properties of Ni ferrite nanocrystals dispersed in the silica matrix by sol-gel technique", *J. Magn. Mater.*, 281: 234-239.

3. Manouchehri, S., Yousefi, M. H., Mozaffari, M., Amighian, J. (2010). "Preparation of Superparamagnetic of $\text{Co}_{0.5}\text{Zn}_{0.5}\text{Fe}_2\text{O}_4$ at Room Temperature by Co-precipitation Method and Investigation of Its Physical Properties", *Int. J. Nanosci. Nanotechnol.*, 6: 15-22.
4. Wang, H. Zhang, F., Zhang, W., Wang, X., Lu, Z., , Qian, Z., Sui, Y., Dong, D., Su, W. (2006). "The effect of surface modification on the morphology and magnetic properties of NiFe_2O_4 nanoparticles", *J. Cryst. Growth*, 293: 169–174.
5. Khairy, M. (2014). "Synthesis, characterization, magnetic and electrical properties of polyaniline/ NiFe_2O_4 nanocomposite", *Synthetic Met.*, 189: 34– 41.
6. Prabhakaran, T., Hemalatha, J. (2011). "Combustion synthesis and characterization of highly crystalline single phase nickel ferrite nanoparticles", *J. Alloys Compd.*, 509: 7071–7077.
7. Mozaffari, M. Aboalizadeh, Z., Amighian, J. (2011). "Investigation of magnetic properties of Al substituted nickel ferrite nanopowders synthesized by the sol-gel method", *J. Magn. Magn. Mater.*, 323: 2997-3000.
8. Maaz, K., Karim, S., Mumtaz, A., Hasanain, S.K., Liu, J., Duan, J.L. (2009) "Synthesis and magnetic characterization of nickel ferrite nanoparticles prepared by co-precipitation route", *J. Magn. Magn. Mater.*, 321: 1838–1842.
9. Komarneni, S., D'Arrigo, M. C., Leonelli, C, Pellacani G. C., Katsuki, H. (1998). "Microwave-Hydrothermal Synthesis of Nanophase Ferrites", *J. Amer. Ceram. Soc.*, 81: 3041.
10. Alamolhoda, S. Mirkazemi, S. M., Shahjooyi, T., Benvidi, N. (2015). "Effect of Cetyl trimethyl ammonium bromide (CTAB) amount on phase constituents and magnetic properties of nano-sized NiFe_2O_4 powders synthesized by sol-gel auto-combustion method", *J. Alloys Compd.*, 638: 121-136.
11. George, M, John, A. M., Nair, S. S., Joy, P. A., Anantharaman, M. R. (2006). "Finite size effects on the structural and magnetic properties of sol-gel synthesized NiFe_2O_4 powders", *J. Magn. Magn. Mater.*, 302:190–195.
12. Sivakumar, P., Ramesh, R., Ramanand, A., Ponnusamy, S., Muthamizhchelvan, C. (2012). "Structural, thermal, dielectric and magnetic properties of NiFe_2O_4 nanoleaf", *J. Alloys Compd.*, 537: 203–207.
13. Cullity, B. D. (1978). "*Elements of X-ray Diffraction*", second ed., Addison-Wesely Publishing Co.
14. Shokrollahi, H., Janghorban, K. (2007). "Review: Influence of additives on the magnetic properties microstructure and densification of Mn-Zn soft ferrites", *Mater. Sci. Eng. B*, 141: 91-107.
15. Raghavender, A. T. Biliškov, N., Skoko, Ž. (2011). "XRD and IR analysis of nanocrystalline Ni-Zn ferrite synthesized by the sol-gel method", *Mater. Lett.*, 65: 677–680.
16. Costa, A. C. F. M., Silva, V. J., Cornejo, D. R., Morelli, M. R., Kiminami, R. H. G. A., Gama, L. (2008). "Magnetic and structural properties of NiFe_2O_4 ferrite nanopowder doped with Zn^{2+} ", *J. Magn. Magn. Mater.*, 320: 370-372.
17. Tan, X., Li, G., Zhao, Y., Hu, C. (2009). "The effect of Cu content on the structure of $\text{Ni}_{1-x}\text{Cu}_x\text{Fe}_2\text{O}_4$ spinels", *Mater. Res. Bull.*, 44: 2160-216.
18. Rietveld, H. M. (1969). "A profile refinement method for nuclear and magnetic structures", *J. Appl. Cryst.*, 2: 65–71.
19. Tsay, C. Y., Fan, K. S., Lei, C. M. (2012). "Synthesis and characterization of sol-gel derived gallium-doped zinc oxide thin films", *J. Alloys Compd.*, 512: 216– 222.
20. Bahadur N., Jain, K, Srivastava, A. K., Govind, Gakhar, R, Haranath, D., Dulat, M. S. (2010). "Effect of nominal doping of Ag and Ni on the crystalline structure and photo-catalytic properties of mesoporous titania", *Mater. Chem. Phys.*, 124: 600–608.
21. Iqbal M. J., Ashiq M. N. (2007). "Comparative studies of $\text{SrZr}_x\text{Mn}_x\text{Fe}_{12-2x}\text{O}_{19}$ nanoparticles synthesized by co-precipitation and sol-gel combustion methods", *Scripta Mater.*, 56: 145–148.
22. Sivakumar, P., Ramesh, R., Ramanand, A., Ponnusamy, S., Muthamizhchelvan, C. (2011). "Preparation and properties of nickel ferrite (NiFe_2O_4) nanoparticles via sol-gel auto-combustion method", *Mater. Res. Bull.*, 46: 2204–2207.
23. Tangcharoen, T., Ruangphanit, A., Pecharapa, W. (2013). "Structural and magnetic properties of nanocrystalline zinc-doped metal ferrites (metal=Ni,Mn,Cu) prepared by sol-gel combustion method", *Ceram. Int.*, 39: S239-S243.
24. Néel, L. (1948). "Magnetic properties of fentes: ferrimagnetism and antiferromagnetism", *Ann. Phys. Paris*, 3: 137-198.
25. Shannon, R. D., Prewitt, C. T. (1969). "Effective Ionic Radii in Oxides and Fluorides", *Acta Cryst.*, B25: 925-946.
26. Dimri, M. C. Verma, A., Kashyap, S. C., Dube, D. C., Thakur, O. P., Prakash, C., (2006). "Structural, dielectric and magnetic properties of NiCuZn ferrite grown by citrate precursor method", *Mater. Sci. Eng. B*, 133: 42–48.
27. Zhang, H. E., Zhang, B. F., Wang, G. F., Dong, X. H., Gao, Y., (2007). "The structure and magnetic properties of $\text{Zn}_{1-x}\text{Ni}_x\text{Fe}_2\text{O}_4$ ferrite nanoparticles prepared by sol-gel auto-combustion", *J. Magn. Magn. Mater.*, 312: 126–130.

28. Shirsath S. E., Toksha, B. G., Kadam, R. H., Patange, S. M., Mane, D. R., Jangam, S. G., Ghasemi, A., (2010). "Doping effect of Mn^{2+} on the magnetic behavior in Ni–Zn ferrite nanoparticles prepared by sol–gel auto-combustion", *J. Phys. Chem. Solids* 71: 1669–1675.